AGU PUBLICATIONS

JGR

Journal of Geophysical Research: Planets

RESEARCH ARTICLE
10.1002/2016JE005158

Key Points:
- Silicon carbide would be stable in the mantles of Earth-size Si-rich carbide exoplanets
- The thermal expansion parameter of SiC is greater than that of Mg-silicate at high pressure
- Thermal convection may play a more important role at greater depths in Si-rich carbide planets than silicate planets

Supporting Information:
- Supporting Information S1

Correspondence to:
S.-H. Shim,
SHDShim@asu.edu

Citation:
Nisr, C., Y. Meng, A. A. MacDowell, J. Yan, V. Prakapenka, and S.-H. Shim (2017), Thermal expansion of SiC at high pressure-temperature and implications for thermal convection in the deep interiors of carbide exoplanets, *J. Geophys. Res. Planets*, *122*, 124–133, doi:10.1002/2016JE005158.

Received 19 AUG 2016
Accepted 3 JAN 2017
Accepted article online 9 JAN 2017
Published online 14 JAN 2017

Thermal expansion of SiC at high pressure-temperature and implications for thermal convection in the deep interiors of carbide exoplanets

C. Nisr[1], Y. Meng[2], A. A. MacDowell[3], J. Yan[3], V. Prakapenka[4], and S.-H. Shim[1]

[1]School of Earth and Space Exploration, Arizona State University, Tempe, Arizona, USA, [2]High Pressure Collaborative Access Team (HPCAT), Geophysical Laboratory, Carnegie Institution of Washington, Argonne, Illinois, USA, [3]Advanced Light Source, Lawrence Berkeley National Laboratory, Berkeley, California, USA, [4]GSECARS, University of Chicago, Chicago, Illinois, USA

Abstract Recent astrophysical observations have shown that some stars have sufficiently high carbon-to-oxygen ratios and may host planets composed mainly of carbides instead of silicates and oxides. From the low thermal expansion of SiC at 1 bar, it can be inferred that the buoyancy force of thermal anomalies is much lower in the carbide planets than in the silicate planets. However, numerous studies have shown that high pressure in planetary interiors can fundamentally change the physical properties of materials. We have measured the pressure-volume-temperature relations of two SiC polymorphs (3C and 6H) at pressures and temperatures up to 80 GPa and 1900 K and 65 GPa and 1920 K, respectively, in the laser-heated diamond anvil cell combined with synchrotron X-ray diffraction. We found no evidence of dissociations of these phases up to our maximum pressure condition, supporting the stability of SiC to 1900 km depth in Earth-size Si-rich carbide planets. Following the Mie-Grüneisen approach, we fit our data to the Birch-Murnaghan or the Vinet equations of state combined with the Debye approach. We found that the pressure-induced change in the thermal expansion parameter of SiC is much smaller than that of Mg silicate perovskite (bridgmanite). Our new measurements suggest that the thermal buoyancy force may be stronger in the deep interiors of Si-rich carbide exoplanets than in the "Earth-like" silicate planets.

1. Introduction

Surveys have shown that some exoplanet hosting stars have unusually high carbon-to-oxygen ratios (well above 1) [*Bond et al.*, 2010; *Petigura and Marcy*, 2011; *Hinkel et al.*, 2014, 2016]. The measurement of the C/O ratio is however difficult, and some studies have raised questions regarding the abundance of those stars [*Fortney*, 2012; *Nissen*, 2013; *Jura and Young*, 2014; *Teske et al.*, 2014]. Such high carbon-to-oxygen ratios would change the mineral phases precipitating from protoplanetary disks, i.e., carbides instead of silicates, resulting in the formation of carbide planets [*Larimer*, 1975; *Lodders*, 2003; *Bond et al.*, 2010; *Madhusudhan et al.*, 2012; *Unterborn et al.*, 2014] that may contain graphite, CaS, Fe_3C, SiC, and TiN [*Larimer*, 1975]. Silicon carbide (SiC) may be the abundant phase in the deep interiors of such planets or at least it can be used as a proxy in exploring the physical property differences between carbides and silicates [*Larimer*, 1975]. Because carbide-type planets do not exist in our solar system, there are no direct observations for the geophysics and surface tectonics of this potential class of planets. Therefore, alternative approaches, such as laboratory experiments and geodynamic modeling, are particularly important for understanding the geophysics of the carbide exoplanets.

From the studies of numerous mineral phases related to the Earth's interior, geophysicists have learned that high pressure has fundamental impacts on the materials properties. Among many important properties, the density plays an important role in the convection in the deep planetary layers. Pressure-volume-temperature (*P-V-T*) equations of state (EOS) of planetary materials in particular allow us to estimate the density at the *P-T* conditions related to the interiors. In addition, depth-dependent (or pressure-dependent) changes in the thermoelastic properties, which impact the thermal convection, can be derived from the *P-V-T* EOS [*Jackson and Rigden*, 1996].

Although few studies have been conducted for measuring the EOS of SiC polymorphs [*Bassett et al.*, 1993; *Zhuravlev et al.*, 2013], existing studies have focused on the compressibility at 300 K. The thermal parameter

has been estimated through Raman spectroscopy [*Zhuravlev et al.*, 2013]. However, it does not provide how the density changes at high *P-T* directly. Here we report the *P-V-T* relations for two SiC polymorphs measured by combining synchrotron X-ray diffraction (XRD) together with the laser-heated diamond-anvil cell (LHDAC) technique.

2. Experimental Methods

We used pure synthetic SiC samples (Alfa, purity 99.8%) in two different crystal structures: a cubic β phase (hereafter 3C-SiC) and a hexagonal α phase (hereafter 6H-SiC). The purity of the starting materials was examined using XRD and scanning electron microscope (SEM). We found no evidence for impurities and other polymorphs in the starting materials (Figure S1 in the supporting information). Powdered forms of the samples were mixed separately with gold powder that was used as both an internal pressure standard [*Fei et al.*, 2007; *Yokoo et al.*, 2009; *Dorogokupets and Dewaele*, 2007] and a laser coupler. The powder mixtures were cold pressed into thin foils of approximately $60 \times 60\ \mu m^2$ in size and 10 μm in thickness. The thin foils were loaded in a 100 and 260 μm diameter hole drilled in a rhenium gasket indented by diamond anvils with 200 and 400 μm diameter culets, respectively. Three to four spacer particles of the sample material (<10 μm) were added on each culet to separate the foil from the diamond anvils to allow the pressure medium to form layers between the sample foil and the diamond anvils for thermal insulation and to prevent large thermal gradients during laser heating. We loaded neon as a pressure transmitting medium using the gas-loading system at GSECARS [*Rivers et al.*, 2008] for 12 of the 13 synchrotron XRD runs we performed. For one of the runs that represents 4% of the room temperature data and 24% of the high-temperature data, we cryogenically loaded argon as a pressure medium using the loading system at the high-pressure laboratory at Arizona State University. The data obtained from the runs with neon and argon agreed well with each other.

Synchrotron XRD patterns were measured in situ at high *P-T* in double-sided LHDAC at the beamline 16-IDB of the High Pressure Collaborative Access Team (HPCAT) sector at the Advanced Photon Source, at the beamline 12.2.2 at the Advanced Light Source (ALS), and at the 13-IDD beamline of the GeoSoilEnviroConsortium for Advanced Radiation Sources (GSECARS) sector at the Advanced Photon Source. Monochromatic X-ray beams (wavelengths of 0.3515, 0.4133, and 0.3344 Å at HPCAT, ALS, and GSECARS, respectively) were focused on the sample, and we collected diffraction images on a MarCCD detector while compressing 3C-SiC and 6H-SiC up to ~75 and ~65 GPa, respectively. Near-infrared laser beams were coaxially aligned with the X-ray beam and focused on the samples for an in situ heating. We have heated the samples at 1600–2200 K after compression to several different pressures. Temperatures are estimated by fitting the measured thermal radiation spectra to the Plank equation for both sides of the samples in LHDAC.

We integrated the diffraction images to the 1-D diffraction patterns using DIOPTAS [*Prescher and Prakapenka*, 2015]. Distortions and the detector distance (~200 mm) were calibrated and then corrected from the data during the integration by using the CeO_2 and LaB_6 standards. We then fit the diffraction peaks with a pseudo-Voigt profile function to obtain the peak positions. We determined the pressure from the measured unit cell volume of gold combined with its EOS [*Fei et al.*, 2007; *Yokoo et al.*, 2009; *Dorogokupets and Dewaele*, 2007]. We used the obtained peak positions of SiC to refine the unit cell parameters using the UnitCell software [*Holland and Redfern*, 1997]. Our pressure-volume-temperature data are provided in the supporting information (Tables S1–S8).

3. Results and Discussions

3.1. High-Temperature Stability of SiC

It is of interest if SiC is stable or breaks down to Si and C at simultaneous high *P* and *T* relevant to the conditions expected for planetary interiors. The pressure conditions can be calculated from the size and the mass of planets. However, the temperature is much more difficult to estimate because it is highly dependent on the formation processes, the evolutionary paths, and the ages of planets. If we assume that carbide planets would have similar temperature structures as that of Earth, our temperature conditions are applicable for testing the stability of SiC in the interiors of carbide exoplanets. It is also notable that for Earth-size planets, the density is much more affected by the pressure than by the temperature [*Jeanloz*, 1989].

We did not find any changes in the diffraction patterns during and after the laser heating process up to 2200 K for a duration of ~14 min. We did not find any changes related to (1) the dissociation of SiC to Si and C and

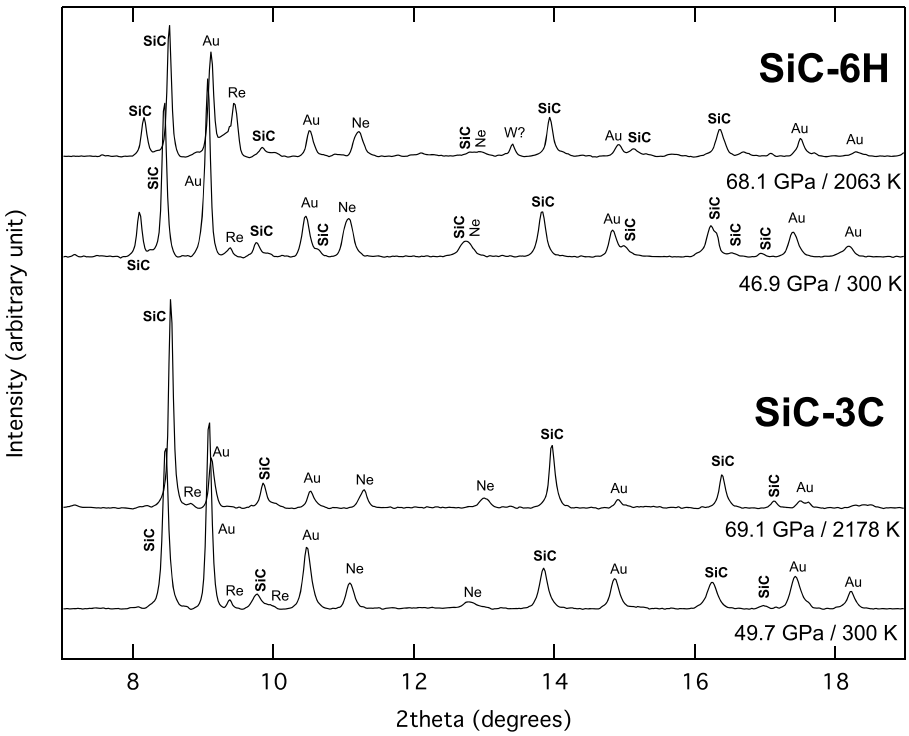

Figure 1. X-ray diffraction patterns of 3C-SiC and 6H-SiC at high pressures and temperatures. Au, gold as an internal pressure standard and laser coupler; Re, rhenium gasket; Ne, neon as a pressure transmitting medium and thermal insulator; W?, unknown single dot observed only in a few diffraction images of 6H-SiC (although the position coincides with that of W, possibly from loading needle, because no other lines are observed, the assignment remains tentative).

(2) a phase transition in SiC at pressures between 1 and 80 GPa and temperatures between 1600 and 2200 K (Figure 1).

We did not observe any sign of phase transition from 3C to 6H or from 6H to 3C. At very low pressure, we found that 6H (lower-pressure, higher-temperature phase) may transform to 3C (higher-pressure, lower-temperature phase), at 2.5 GPa and 2173 K with a positive Clapeyron slope, suggesting that 3C would be the stable form at pressures higher than 6 GPa. However, the possible phase transition was identified only through appearance of a few lines and no complete phase transition was observed in the XRD measurements.

During our in situ measurements on 3C as a starting material, we reached temperatures of ~2200 K at several pressure points. However, we did not observe new diffraction lines, suggesting that there is no transition from 3C to 6H within the *P*–*T* range we explored, being consistent with *Sugiyama and Togaya* [2001] in that 3C may be stable at the *P-T* conditions. However, in our in situ measurements with 6H as a starting material, we did not find any evidence of a phase transition from 6H to 3C.

Through first-principle calculations, *Park et al.* [1994] showed that the free energy differences among SiC polymorphs are very small. If the kinetic barrier for inducing the phase transition from 6H to 3C is large at high *P*, it may be difficult to observe the phase transition. *Sekine and Kobayashi* [1997] conducted shockwave experiments for 6H-SiC and did not find any evidence for the 6H-to-3C transition within the resolution of their data other than a phase transition to rocksalt structure at 105 GPa. However, because the density difference between 3C and 6H is very small and the shockwave techniques do not measure the structure directly, the study does not rule out the possibility of a transition. Therefore, it remains uncertain which of 3C and 6H is more stable at the *P-T* range that we explored due to the experimental difficulties. However, our results support that Si remains to be fourfold coordinated in SiC within the explored *P-T* range.

3.2. Equation of State

Because gold is widely used as an internal pressure standard in high-pressure experiments, numerous efforts have been made to improve its EOS. However, the existing studies have shown significant discrepancies in the thermal pressure term of its EOS. We conducted EOS fittings for our data using a range of different EOSs of

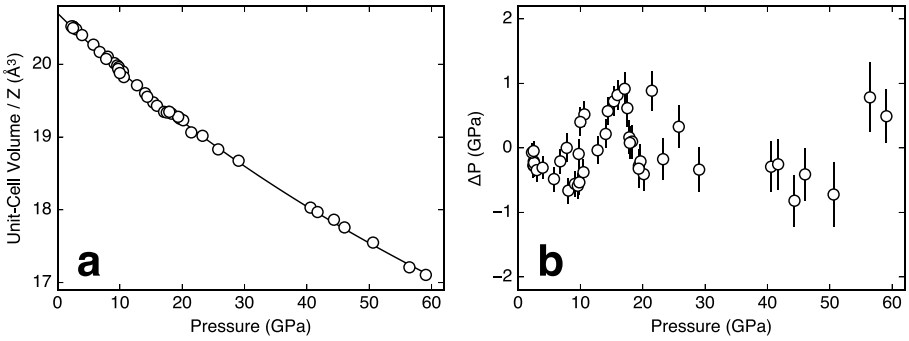

Figure 2. Results for the equation of state fit for 3C-SiC at 300 K using the gold scale by *Dorogokupets and Dewaele* [2007]. (a) Pressure-volume relations (unit cell volume divided by the number of formula unit) and (b) fit residue in pressure. An isotherm in Figure 2a is obtained from the fitting result. The error bars represent the 1σ uncertainty estimated from the measured uncertainties in volumes.

gold [*Fei et al.*, 2007; *Yokoo et al.*, 2009; *Dorogokupets and Dewaele*, 2007], and we present three representative results here.

We follow the Mie-Grüneisen approach where the total pressure, $P_{tot}(V,T)$, is expressed as a sum of the pressure along a reference isotherm, $P_{st}(V,T_0)$ (normally 300 K), and the thermal pressure, $\Delta P_{th}(V,T)$:

$$P_{tot}(V,T) = P_{st}\left(V,T_0\right) + \Delta P_{th}(V,T). \tag{1}$$

For the reference isotherms of 3C and 6H, we fit the pressure-volume data at 300 K to either the Birch-Murnaghan or the Vinet equation of state, depending on the equation used in the EOS of gold. For example, for fittings with the EOSs of gold by *Fei et al.* [2007] and *Yokoo et al.* [2009], we used the third-order Birch-Murnaghan equation [*Birch*, 1978]:

$$P = \frac{3K_0}{2}\left[\left(\frac{V_0}{V}\right)^{7/3} - \left(\frac{V_0}{V}\right)^{5/3}\right]\left\{1 - \xi\left[\left(\frac{V_0}{V}\right)^{2/3} - 1\right]\right\}, \tag{2}$$

where $\xi = \frac{3}{4}\left(4 - K_0'\right)$, K is the bulk modulus, K' is the pressure derivative of the bulk modulus, and subscript 0 represents the reference state (1 bar and 300 K for our case). For the fitting with the gold EOS by *Dorogokupets and Dewaele* [2007], we used the Vinet equation [*Vinet et al.*, 1987] (Figures 2 and 3):

$$P = \frac{3K_0(1-x)}{x^2}\exp[\eta(1-x)], \tag{3}$$

where $x = (V/V_0)^{1/3}$ and $\eta = \frac{3}{2}\left(K_0' - 1\right)$. Because V_0 can be measured directly at the reference conditions, we fixed it to the experimentally measured values. All the EOS fittings in this study were conducted using the MINPACK package [*Moré et al.*, 1980].

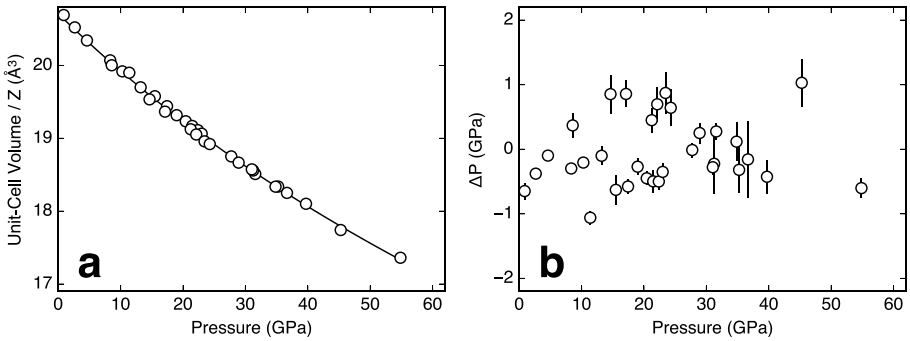

Figure 3. Results for the equation of state fit for 6H-SiC at 300 K using the gold scale by *Dorogokupets and Dewaele* [2007]. (a) Pressure-volume relations (unit cell volume divided by the number of formula unit) and (b) fit residue in pressure. An isotherm in Figure 3a is obtained from the fitting result. The error bars represent the 1σ uncertainty estimated from the measured uncertainties in volumes.

Table 1. Equation of State Fit Results for 3C- and 6H-SiC Using Three Different Equations of State of Gold[a]

Parameters	Au EOS by F07, Y09, D07	References
	3C-SiC	
V_0	82.804 ± 0.027 Å^3	This work[b,d]
K_0	241, 242, 243 ± 5 GPa	This work[c,d]
K_0'	2.84, 2.85, 2.68 ± 0.21	This work[c,d]
γ_0	1.06	*Clayton* [2010][d]
q	−1.25, 0.14, 0.67 ± 0.25	This work
θ_0	1200 K	*Stockmeier et al.* [2009][d]
	6H-SiC	
V_0	124.27 ± 0.01 Å^3	This work[b,d]
K_0	243, 244, 245 ± 5 GPa	This work[c,d]
K_0'	2.79, 2.80, 2.59 ± 0.31	This work[c,d]
γ_0	1.06	*Clayton* [2010][d]
q	−0.77, 0.74, 1.35 ± 0.27	This work
θ_0	1200 K	*Karch et al.* [1996][d]

[a]F07: *Fei et al.* [2007], Y09: *Yokoo et al.* [2009], D07: *Dorogokupets and Dewaele* [2007] .
[b]Fixed during $P-V$ EOS (300 K) fit.
[c]Obtained from $P-V$ EOS fit.
[d]Fixed during $P-V-T$ (high temperature) EOS fit.

As shown in Table 1, within the estimated uncertainty, the bulk modulus (K_0) and its pressure derivative (K_0') are not different between the 3C and the 6H phases of SiC. We also include results from other types of EOS analyses in Figures S2–S5 in the supporting information.

Our fitting results for K_0 are not sensitive to the EOS of gold as shown in Table 1. For K_0', the difference shown in Table 1 is mainly due to the use of different equations for the 300 K isotherm, rather than the effects of different gold EOS. Such differences have been found in the studies of many different materials at high pressure [*Fei et al.*, 2007].

Our K_0 and K_0' values obtained using the EOS of gold by *Fei et al.* [2007] are consistent with those obtained by *Zhuravlev et al.* [2013] for 3C through XRD where the same pressure scale was used (Table 2). However, our values are different from their Brillouin spectroscopy measurements. Although Brillouin spectroscopy can directly measure K_0 and K_0', fitting *P-V* data to the EOS suffers from a negative correlation between K_0 and K_0' when they are both included in the fitting [*Bell et al.*, 1987]. Indeed, if we fix K_0 to their Brillouin value, we obtain the same K_0' as theirs. However, because the study by *Zhuravlev et al.* [2013] does not provide a complete thermal EOS, we decided to use the fitting results constrained by the full thermal EOSs of gold [*Fei et al.*, 2007; *Yokoo et al.*, 2009; *Dorogokupets and Dewaele*, 2007]. This choice does not impact our main conclusion because the difference between *Zhuravlev et al.*'s [2013] Brillouin and our results is essentially because of the trade-off between the fit parameters, not because of the difference in compressional behavior itself. Our values are different from those reported by earlier studies [*Strössner et al.*, 1987; *Bassett et al.*, 1993; *Yoshida et al.*, 1993; *Amulele et al.*, 2004] (Table 2). Compared with these studies, we made improvements in reducing deviatoric stresses and expanding the pressure range.

Table 2. Bulk Modulus and Pressure Derivative of Bulk Modulus of 3C- and 6H-SiC[a]

References	K_0 (GPa)	K_0'	Technique
	3C-SiC		
Yoshida et al. [1993]	260(9)	2.9(1)	XRD
Strössner et al. [1987]	248(9)	4.0(3)	XRD
Zhuravlev et al. [2013]	240(9)	3.0(2)	XRD[c]
Zhuravlev et al. [2013]	218(1)	3.75(4)	Brillouin[c]
	6H-SiC		
Bassett et al. [1993]	230(4)	4[b]	XRD
Amulele et al. [2004]	217(1)	4.19(9)	Ultrasonic
Amulele et al. [2004]	218(5)	4.19(9)	XRD

[a]Fixed during fitting.
[b]Based on the Ne scale by *Fei et al.* [2007].
[c]Direct integration from Brillouin data.

We fit the volume data at high *P-T* through the Mie-Grüneisen-Debye approach:

$$\Delta P_{\mathrm{th}}(V,T) = \frac{\gamma(V)}{V}\Delta E_{\mathrm{th}}[\theta(V),T], \quad (4)$$

where θ is the Debye temperature and γ is the Grüneisen parameter. The internal energy change (ΔE_{th}) can be calculated from the Debye model:

$$E_{\mathrm{th}} = \frac{9nRT}{z^3}\int_0^z \frac{\xi^3}{e^{\xi}-1}\mathrm{d}\xi, \quad (5)$$

where R is the gas constant, z is θ/T, and n is the number of atoms per formula unit. For the volume-dependent changes, we assumed

$$\gamma = \gamma_0\left(\frac{V}{V_0}\right)^q \quad (6)$$

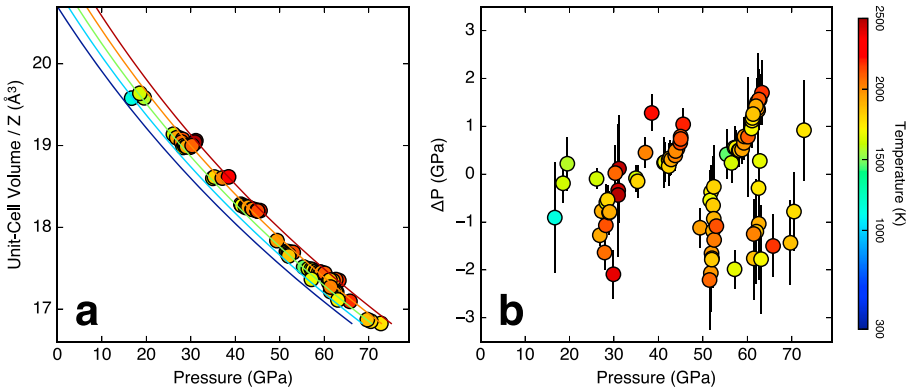

Figure 4. Results for the equation of state fit for 3C-SiC at high temperature using the gold scale by *Dorogokupets and Dewaele* [2007]. (a) Pressure-volume relations (unit cell volume divided by the number of formula unit) and (b) fit residue in pressure. The error bars represent the 1σ uncertainty estimated from the measured uncertainties in volumes and temperatures. Isotherms in Figure 4a are obtained from the fitting result. The symbols and the isotherms are color coded to temperature.

where q is the logarithmic volume dependence of γ. Then the volume dependence of θ can be obtained from

$$\theta = \theta_0 \exp\left(\frac{\gamma_0 - \gamma}{q}\right). \tag{7}$$

We fit the data to either the Vinet–Debye (Figures 4 and 5) or Birch-Murnaghan-Debye EOS (Figures S6 and S7) depending on the used EOS of gold. In the fitting, we fixed V_0, γ_0, and θ_0 to the values measured at 1 bar. We also fixed K_0 and K_0' to the values we obtained by fitting our *P-V* data at 300 K. We calculated γ_0 from the heat capacity, the thermal expansion parameter, the bulk modulus, and the density measured at 1 bar using thermodynamic relations [*Müller et al.*, 1998; *Stockmeier et al.*, 2009; *Clayton*, 2010]. The used thermodynamic Grüneisen parameter is in agreement with the Grüneisen parameter estimated from Raman spectroscopy [*Zhuravlev et al.*, 2013]. Therefore, the only parameter that was varied during the fitting was the logarithmic volume dependence of the Grüneisen parameter, q. This parameter informs us essentially on the pressure-dependent changes in the thermal pressure (αK_T) and the thermal expansion parameter (α).

We found that q is particularly sensitive to the choice of the EOS of gold (Table 1). Among the EOSs of gold we tried, the largest q value was obtained when the EOS of gold by *Dorogokupets and Dewaele* [2007] was used. The EOS of gold by *Fei et al.* [2007] yields negative q value, which is rare but not impossible [*Kumari and Dass*, 1986]. The EOSs by *Yokoo et al.* [2009] and *Dorogokupets and Dewaele* [2007] include the anharmonic effects and electronic effects, while *Fei et al.* [2007] used a quasi-harmonic approximation without electronic effects.

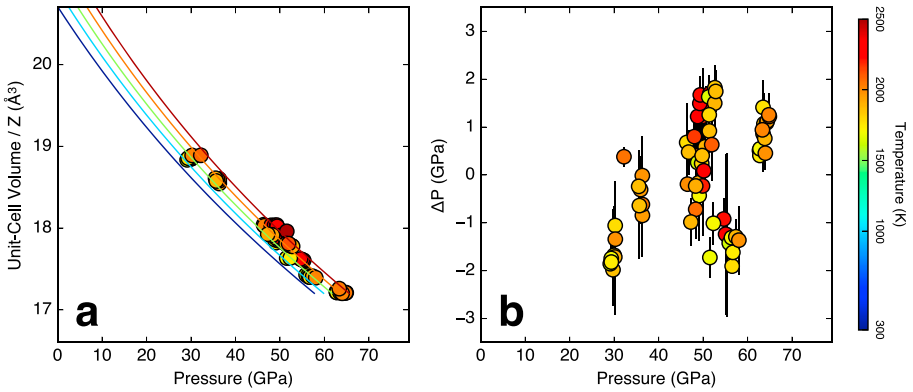

Figure 5. Results for the equation of state fit for 6H-SiC at high temperature using the gold scale by *Dorogokupets and Dewaele* [2007]. (a) Pressure-volume relations (unit cell volume divided by the number of formula unit) and (b) fit residue in pressure. The error bars represent the 1σ uncertainty estimated from the measured uncertainties in volumes and temperatures. Isotherms in Figure 5a are obtained from the fitting result. The symbols and the isotherms are color coded to temperature.

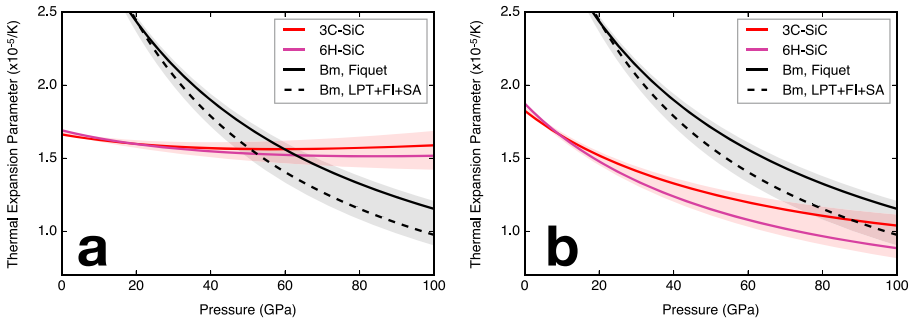

Figure 6. The thermal expansion parameters of Mg silicate perovskite (bridgmanite; black solid and dashed curves), 3C-SiC (red curve), and 6H-SiC (magenta curve) at high pressure and 2500 K. The light red shaded area represents the estimated 1σ uncertainty. For bridgmanite, we present the thermal expansion parameter from *Fiquet et al.* [1998, 2000] based on LHDAC and *Shim and Duffy* [2000] where multiples of data sets are inverted together [*Ross and Hazen*, 1989; *Wang et al.*, 1994; *Utsumi et al.*, 1995; *Funamori et al.*, 1996; *Saxena et al.*, 1999; *Fiquet et al.*, 1998]. Other recent results such as *Tange et al.* [2012] lie within the range shown by the gray area. We present the thermal expansion parameter of SiC obtained using the gold scale by *Fei et al.* [2007] in Figure 6a and by *Dorogokupets and Dewaele* [2007] in Figure 6b.

However, due to the lack of absolute pressure measurements for gold at a sufficient *P-T* range, it remains uncertain which EOS of gold is more reliable.

In order to estimate the impact of the high-pressure behaviors of SiC on the thermal convection of planets, we calculated the thermal expansion parameter (α) as a function of pressure along with an isotherm (2500 K). We present the two most extreme cases from our fitting results in Figure 6. The negative q obtained using the gold EOS by *Fei et al.* [2007] results in no changes in the thermal expansion parameter of SiC with pressure. In the case of the fitting result obtained from the gold EOS by *Dorogokupets and Dewaele* [2007], the high q results in a decrease in the thermal expansion parameter of SiC with pressure.

We also compared it with the thermal expansion parameter of bridgmanite ($MgSiO_3$) [*Ross and Hazen*, 1989; *Wang et al.*, 1994; *Utsumi et al.*, 1995; *Funamori et al.*, 1996; *Fiquet et al.*, 1998; *Saxena et al.*, 1999; *Fiquet et al.*, 2000; *Shim and Duffy*, 2000; *Stixrude and Lithgow-Bertelloni*, 2005; *Tange et al.*, 2012], which is the most dominant mineral phase in the Earth's lower mantle, at the same *P-T* conditions. While the thermal expansion parameter of bridgmanite is known to decrease strongly with pressure, according to our measurements, the thermal expansion parameter of SiC does not decrease at all with pressure (for the case with the gold EOS by *Fei et al.* [2007]) or decreases much more gently with pressure (for the case with the gold EOS by *Dorogokupets and Dewaele* [2007]). Although the thermal expansion parameter of SiC is much smaller than bridgmanite at lower pressures, it becomes similar or even greater than that of bridgmanite at higher pressures.

Because the buoyancy force is proportional to the thermal expansion parameter in the isochemical case, the difference in the pressure-dependent changes of the thermal expansion parameter that we found implies that a thermally driven mantle convection would be different in carbide exoplanets when compared with silicate planets, like Earth. Although carbide planets would have much less thermal buoyancy force for temperature anomalies than silicate planets at shallow depths, the no or smaller decrease in the thermal expansion parameter of SiC with depth would make the thermally driven flow more vigorous in the deep interiors of carbide planets than in silicate planets.

4. Conclusions and Implications

Our high-pressure experiments show that a fourfold coordinated Si (3C or 6H) would remain stable up to 80 GPa and 2200 K in SiC without dissociation to Si and C. Both static and dynamic compression studies have shown a phase transition to a rocksalt-type structure (B1, where Si is sixfold coordinated by C) from 6H- and 3C-SiC (where Si is fourfold coordinated by C) at ~105 GPa [*Yoshida et al.*, 1993; *Sekine and Kobayashi*, 1997]. Therefore, in an Earth-sized Si-rich carbide planet (with a similar Fe core size as shown in Figure 7), a fourfold coordinated Si would be stable to ~2300 km depth ($R/R_\oplus \simeq 0.63$). It is notable that a fourfold coordinated Si disappears at a much shallower depth in the Earth's interior (i.e., 660 km, $R/R_\oplus = 0.89$) [*Ito and Takahashi*, 1989; *Shim et al.*, 2001].

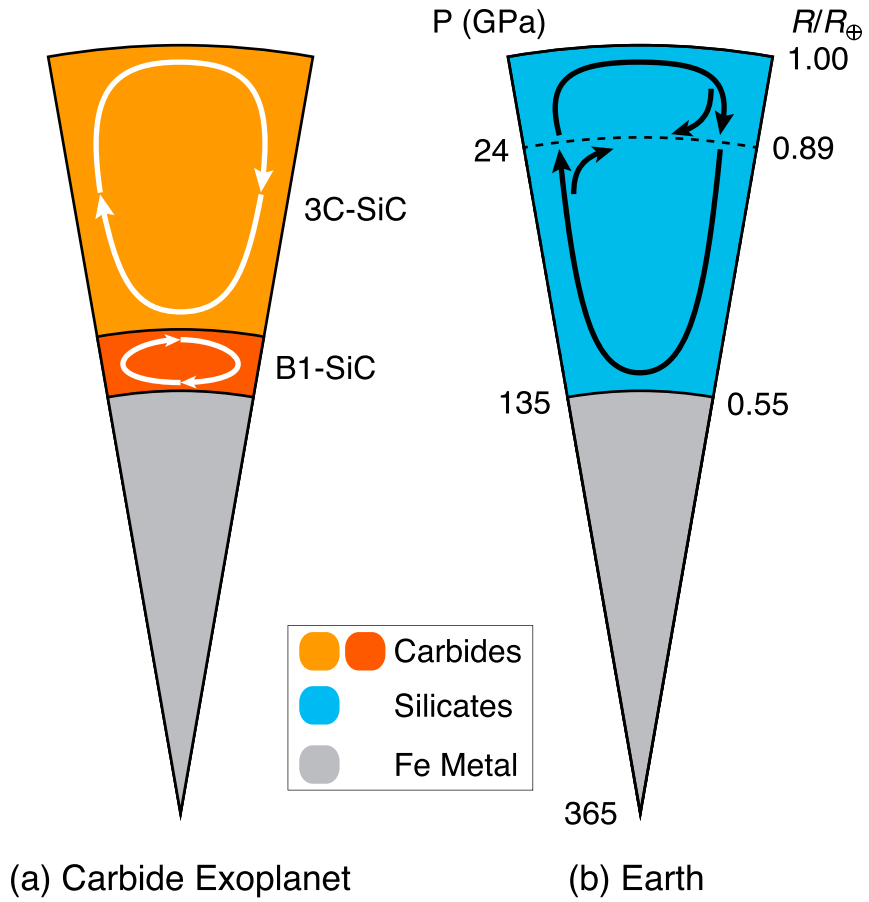

Figure 7. Possible internal structure and dynamics of (a) a carbide-type planet with low Mg/Si ratio (assumed Earth-size) compared with those of (b) Earth. The arrows indicate the scale of thermal convection in the mantle.

Our high-pressure experiments indicate that the thermal expansion parameter of SiC, a likely stable phase in the outermost 2300 km thick layer of an Earth-sized carbide planet, is much less sensitive to the pressure (i.e., depth) compared with that of silicates (Figure 6). Although the lower thermal expansion parameter of SiC at lower pressures would make the thermal buoyancy force lower at shallower depths compared with Earth, the little to no decrease seen in the thermal expansion parameter of SiC with depth would make the thermal buoyancy force a much more important factor to consider for the deep mantle convection in carbide planets.

As discussed before, a phase transition in SiC to a B1 structure would produce a discontinuity in the deep carbide mantle (Figure 7). Some phase transitions with an increase in the Si coordination number, for example, the post-spinel and post-ilmenite transition at 660 km depth in the Earth's interior, are known to have negative phase boundary (Clapeyron) slopes [*Navrotsky*, 1980; *Ito and Takahashi*, 1989; *Shim et al.*, 2001]. As shown by numerous dynamic studies [e.g., *Christensen and Yuen*, 1985; *Tackley et al.*, 1993], such negative phase boundary slopes can stagnate thermal flows across the boundaries. Although there is no direct measurements on SiC, materials with the same crystal structures as 3C- and 6H-SiC (such as ZnO and (Zn,Fe)S) have negative slopes for the same type of phase transition [*Kusaba et al.*, 1999; *Seko et al.*, 2005; *Jiang et al.*, 2007].

The permeability of such phase transitions with an increase in the coordination number for thermal mantle flow is controlled by the magnitude of the slope, and the density increases at the phase transitions [*Christensen and Yuen*, 1985; *Tackley et al.*, 1993]. Although it is unknown for SiC, for example, (Zn,Fe)S has a slope as large (in magnitude) as $-12 \sim -16$ MPa/K for the same type of phase transition. This is a factor of 5–10 greater than the postspinel boundary which is believed to be responsible for the 660 km discontinuity in the Earth [*Irifune et al.*, 1998; *Shim et al.*, 2001; *Ye et al.*, 2014]. The 660 km discontinuity in the Earth appears to be a partially permeable boundary for the mantle flow [*Tackley et al.*, 1993; *Van der Hilst et al.*, 1997]. While the density increase at the 660 km depth in Earth is ~5% [*Shearer and Flanagan*, 1999], it increases to as much

as 15–20% for the phase transition to a B1 structure in SiC [*Yoshida et al.*, 1993; *Sekine and Kobayashi*, 1997]. Therefore, the impact for the thermal mantle flow is expected to be much greater for the coordination number change in Si from 4 to 6 in SiC in a carbide planet than in silicates in a silicate planet (e.g., Earth), suggesting a little to a no thermal flow across the deep phase boundary in a carbide planet, i.e., layered convection. Such limited flow has important implications for the geochemical cycle of volatiles (such as water and carbon) and for the thermal evolution of the planet. As those factors likely affect the surface environment, combined with different crustal compositions expected for carbide planets, the evolutionary path of the surface environment of carbide planets would be significantly different from that of silicate planets, including Earth.

It is important to mention that there are also other important factors to consider in order to understand the internal dynamics and structure of carbide planets. Vigor of mantle convection can be estimated from the Rayleigh number (ratio of buoyancy to diffusion) [*Wolstencroft et al.*, 2009], which can be defined as

$$Ra_H = \frac{\rho^2 g \alpha d^5 A}{k \kappa \eta}, \tag{8}$$

where ρ is the density, g is the gravitational acceleration, α is the thermal expansion parameter, d is the distance, A is the heat production per unit mass, k is the coefficient of thermal conductivity, κ is the thermal diffusivity, and η is the dynamic viscosity. For example, the Earth's mantle has a value on the order of 10^9 [*Wolstencroft et al.*, 2009]. The thermal conductivity of SiC (300–400 W/(m K)) [*Li et al.*, 1998] is known to be much greater than those of silicates (1–2 W/(m K)), which may make the conductive heat transfer a much more important process in Si-rich carbide exoplanets than in silicate planets and reduces the Rayleigh number significantly in the carbide planets. However, it is unknown how the thermal conductivity of SiC changes with pressure. Although viscosity is an important parameter for internal dynamics of planets, the viscosity of SiC at high pressure is not well known. The comparison of the thermal expansion parameter we made in this study considers the effects of the pressure because the temperature effects tend to be smaller. However, it is also important to mention that the thermal evolution and structure of the carbide exoplanets could be very different from those of silicate planets. In addition, in our discussion above, we assumed that SiC is the main constituent of some carbide planets, which would be the case for low Mg/Si ratio planets with high C/O ratios. Because other elements should exist in the carbide planets, future experiments and computations should explore the phase relations and physical properties of carbides in multicomponent systems, such as the Mg-Si-Fe-C system.

Acknowledgments

The results reported herein benefitted from collaborations and/or information exchange within NASA's Nexus for Exoplanet System Science (NExSS) research coordination network sponsored by NASA's Science Mission Directorate. We thank two anonymous reviewers and the Editor for the helpful discussions. C. Nisr is also supported by NSF (EAR1321976). Portions of this work were performed at GSECARS (University of Chicago, Sector 13) and HPCAT (Sector 16), APS, ANL, and beamline 12.2.2., ALS, LBNL. GSECARS is supported by the NSF (EAR-1128799) and DOE (DE-FG02-94ER14466). HPCAT is supported by DOE-NNSA (DE-NA0001974) and DOE-BES (DE-FG02-99ER45775). APS and ALS are U.S. DOE Office of Science User Facilities operated for the DOE Office of Science by ANL and LBNL (DE-AC02-06CH11357 and DE-AC02-05CH11231), respectively. Use of the COMPRES-GSECARS gas loading system was supported by COMPRES (NSFEAR-11-57758) and by GSECARS (NSFEAR-1128799; DOEDE-FG02-94ER14466). Data supporting the figures and conclusions are available within the paper and the Supporting Information. Please contact C. Nisr, carole.nisr@gmail.com or S.-H. Shim, SHDShim@asu.edu regarding access to the raw data.

References

Amulele, G. M., M. H. Manghnani, B. Li, D. J. Errandonea, M. Somayazulu, and Y. Meng (2004), High pressure ultrasonic and x-ray studies on monolithic SiC composite, *J. Appl. Phys.*, *95*(4), 1806–1810.

Bassett, W., M. Weathers, T.-C. Wu, and T. Holmquist (1993), Compressibility of SiC up to 68.4 GPa, *J. Appl. Phys.*, *74*(6), 3824–3826.

Bell, P., H. Mao, and J. Xu (1987), Error analysis of parameter-fitting in equations of state for mantle minerals, in *High-Pressure Research in Mineral Physics: A Volume in Honor of Syun-iti Akimoto*, edited by M. H. Manghnani and Y. Syono, pp. 447–454, AGU, Washington, D. C.

Birch, F. (1978), Finite strain isotherm and velocities for single-crystal and polycrystalline NaCl at high pressures and 300°K, *J. Geophys. Res.*, *83*, 1257–1268.

Bond, J. C., D. P. O'Brien, and D. S. Lauretta (2010), The compositional diversity of extrasolar terrestrial planets. I. In situ simulations, *Astrophys. J.*, *715*(2), 1050–1070.

Christensen, U. R., and D. A. Yuen (1985), Layered convection induced by phase transitions, *J. Geophys. Res.*, *90*, 10,291–10,300.

Clayton, J. D. (2010), A geometrically non-linear model of ceramic crystals with defects applied to silicon carbide (SiC), *ARL-TR-5096*, Army Res. Lab. Aberdeen Proving Ground, Maryland.

Dorogokupets, P. I., and A. Dewaele (2007), Equations of state of MgO, Au, Pt, NaCl-B1, and NaCl-B2: Internally consistent high-temperature pressure scales, *High Pressure Res.*, *27*(4), 431–446.

Fei, Y., A. Ricolleau, M. Frank, K. Mibe, G. Shen, and V. Prakapenka (2007), Toward an internally consistent pressure scale, *Proc. Natl. Acad. Sci. U.S.A.*, *104*(22), 9182–9186.

Fiquet, G., D. Andrault, A. Dewaele, T. Charpin, M. Kunz, and D. Häusermann (1998), P-V-T equation of state of $MgSiO_3$ perovskite, *Phys. Earth Planet. Inter.*, *105*, 21–31.

Fiquet, G., A. Dewaele, D. Andrault, M. Kunz, and T. Le Bihan (2000), Thermoelastic properties and crystal structure of $MgSiO_3$ perovskite at lower mantle pressure and temperature conditions, *Geophys. Res. Lett.*, *27*(1), 21–24.

Fortney, J. J. (2012), On the carbon-to-oxygen ratio measurement in nearby Sun-like stars: Implications for planet formation and the determination of stellar abundances, *Astrophys. J. Lett.*, *747*(2), L27.

Funamori, N., T. Yagi, W. Utsumi, T. Kondo, and T. Uchida (1996), Thermoelastic properties of $MgSiO_3$ perovskite determined by in situ X-ray observations up to 30 GPa and 2000 K, *J. Geophys. Res.*, *101*, 8257–8269.

Hinkel, N. R., F. Timmes, P. A. Young, M. D. Pagano, and M. C. Turnbull (2014), Stellar abundances in the solar neighborhood: The hypatia catalog, *Astrophys. J.*, *148*(3), 54.

Hinkel, N. R., et al. (2016), A comparison of stellar elemental abundance techniques and measurements, *Astrophys. J. Suppl. Ser.*, *226*(1), 4.

Holland, T., and S. Redfern (1997), Unit cell refinement from powder diffraction data; the use of regression diagnostics, *Mineral. Mag.*, *61*(1), 65–77.

Irifune, T., et al. (1998), The postspinel phase boundary in Mg_2SiO_4 determined by in situ X-ray diffraction, *Science*, *279*(5357), 1698–1700.
Ito, E., and E. Takahashi (1989), Postspinel transformations in the system Mg_2SiO_4–Fe_2SiO_4 and some geophysical implications, *J. Geophys. Res.*, *94*, 10,637–10,646.
Jackson, I., and S. M. Rigden (1996), Analysis of P-V-T data: Constraints on the thermoelastic properties of high-pressure minerals, *Phys. Earth Planet. Inter.*, *96*(2), 85–112.
Jeanloz, R. (1989), Physical chemistry at ultrahigh pressures and temperatures, *Annu. Rev. Phys. Chem.*, *40*(1), 237–259.
Jiang, X., W.-G. Zhou, H.-S. Xie, Y.-G. Liu, D.-W. Fan, J. Liu, Y.-C. Li, C.-J. Luo, and M.-N. Ma (2007), Phase transition and EOS of marmatite ($Zn_{0.76}Fe_{0.23}S$) up to 623 K and 17 GPa, *Chin. Phys. Lett.*, *24*, 287–290.
Jura, M., and E. Young (2014), Extrasolar cosmochemistry, *Annu. Rev. Earth Planet. Sci.*, *42*, 45–67.
Karch, K., P. Pavone, A. Mayer, F. Bechstedt, and D. Strauch (1996), First-principles study of thermal properties of 3C SiC, *Physica B*, *219*, 448–450.
Kumari, M., and N. Dass (1986), On the pressure dependence of Grüneisen parameter in solids, *Phys. Status Solidi B*, *133*(1), 101–110.
Kusaba, K., Y. Syono, and T. Kikegawa (1999), Phase transition of ZnO under high pressure and temperature, *Proc. Jpn. Acad., Ser. B*, *75*, 1–6.
Larimer, J. W. (1975), The effect of CO ratio on the condensation of planetary material, *Geochim. Cosmochim. Acta*, *39*(3), 389–392.
Li, J., L. Porter, and S. Yip (1998), Atomistic modeling of finite-temperature properties of crystalline β-SiC: II. Thermal conductivity and effects of point defects, *J. Nucl. Mater.*, *255*(2), 139–152.
Lodders, K. (2003), Solar system abundances and condensation temperatures of the elements, *Astrophys. J.*, *591*(2), 1220.
Madhusudhan, N., K. K. Lee, and O. Mousis (2012), A possible carbon-rich interior in super-Earth 55 Cancri e, *Astrophys. J. Lett.*, *759*(2), L40.
Moré, J. J., B. S. Garbow, and K. E. Hillstrom, (1980), User Guide for MINPACK-1, ANL-80-74, Argonne Natl. Lab., Argonne, Ill.
Müller, S. G., R. Eckstein, J. Fricke, D. Hofmann, R. Hofmann, R. Horn, H. Mehling, and O. Nilsson (1998), Experimental and theoretical analysis of the high temperature thermal conductivity of monocrystalline SiC, *Mater. Sci. Forum*, vol. 264, pp. 623–626, Trans Tech Publ., Zürich, Switzerland.
Navrotsky, A. (1980), Lower mantle phase transitions may generally have negative pressure-temperature slopes, *Geophys. Res. Lett.*, *7*, 709–711.
Nissen, P. E. (2013), The carbon-to-oxygen ratio in stars with planets, *Astron. Astrophys.*, *552*, A73.
Park, C., B.-H. Cheong, K.-H. Lee, and K. Chang (1994), Structural and electronic properties of cubic, 2H, 4H, and 6H SiC, *Phys. Rev. B*, *49*(7), 4485.
Petigura, E. A., and G. W. Marcy (2011), Carbon and oxygen in nearby stars: Keys to protoplanetary disk chemistry, *Astrophys. J.*, *735*(1), 41.
Prescher, C., and V. B. Prakapenka (2015), DIOPTAS: A program for reduction of two-dimensional X-ray diffraction data and data exploration, *High Pressure Res.*, *35*(3), 223–230.
Rivers, M., V. B. Prakapenka, A. Kubo, C. Pullins, C. M. Holl, and S. D. Jacobsen (2008), The COMPRES/GSECARS gas-loading system for diamond anvil cells at the Advanced Photon Source, *High Pressure Res.*, *28*(3), 273–292.
Ross, N., and M. Hazen (1989), Single crystal XRD of Mg-pv from 77 to 400 K, *Phys. Chem. Miner.*, *16*, 415–420.
Saxena, S. K., L. S. Dubrovinsky, F. Tutti, and T. Le Bihan (1999), Equation of state of perovskite ($MgSiO_3$) based on experimentally measured data, *Am. Mineral.*, *84*, 226–232.
Sekine, T., and T. Kobayashi (1997), Shock compression of 6H polytype SiC to 160 GPa, *Phys. Rev. B*, *55*(13), 8034.
Seko, A., F. Oba, A. Kuwabara, and I. Tanaka (2005), Pressure-induced phase transition in ZnO and MgO-ZnO pseudobinary system: A first-principles lattice dynamics study, *Phys. Rev. B*, *72*, 024107.
Shearer, P. M., and M. P. Flanagan (1999), Seismic velocity and density jumps across the 410- and 660-kilometer discontinuities, *Science*, *285*, 1545–1548.
Shim, S.-H., and T. S. Duffy (2000), Constraints on the P-V-T equation of state of $MgSiO_3$ perovskite, *Am. Mineral.*, *85*(2), 354–363.
Shim, S.-H., T. S. Duffy, and G. Shen (2001), The post-spinel transformation in Mg_2SiO_4 and its relation to the 660-km seismic discontinuity, *Nature*, *411*(6837), 571–574.
Stixrude, L., and C. Lithgow-Bertelloni (2005), Thermodynamics of mantle minerals—I. Physical properties, *Geophys. J. Int.*, *162*(2), 610–632.
Stockmeier, M., R. Müller, S. Sakwe, P. Wellmann, and A. Magerl (2009), On the lattice parameters of silicon carbide, *J. Appl. Phys.*, *105*(3), 033511.
Strössner, K., M. Cardona, and W. Choyke (1987), High pressure X-ray investigations on 3C-SiC, *Solid State Commun.*, *63*(2), 113–114.
Sugiyama, S., and M. Togaya (2001), Phase relationship between 3C- and 6H-silicon carbide at high pressure and high temperature, *J. Am. Ceram. Soc.*, *84*(12), 3013–3016.
Tackley, P. J., D. J. Stevenson, G. A. Glatzmaier, and G. Schubert (1993), Effects of an endothermic phase transition at 670-km depth in a spherical model of convection in the Earth's mantle, *Nature*, *361*, 699–704.
Tange, Y., Y. Kuwayama, T. Irifune, K. I. Funakoshi, and Y. Ohishi (2012), P-V-T equation of state of $MgSiO_3$ perovskite based on the MgO pressure scale: A comprehensive reference for mineralogy of the lower mantle, *Nature*, *361*, 699–704.
Teske, J. K., K. Cunha, V. V. Smith, S. C. Schuler, and C. A. Griffith (2014), C/O ratios of stars with transiting hot Jupiter exoplanets, *Astrophys. J.*, *788*(1), 39.
Unterborn, C. T., J. E. Kabbes, J. S. Pigott, D. M. Reaman, and W. R. Panero (2014), The role of carbon in extrasolar planetary geodynamics and habitability, *Astrophys. J.*, *793*(2), 124.
Utsumi, W., N. Funamori, and T. Yagi (1995), Thermal expansivity of $MgSiO_3$ perovskite under high pressures up to 20 GPa, *Geophys. Res. Lett.*, *22*, 1005–1008.
Van der Hilst, R. D., S. Widiyantoro, and E. R. Engdahl (1997), Evidence for deep mantle circulation from global tomography, *Nature*, *386*, 578–584.
Vinet, P., J. Ferrante, J. H. Rose, and J. R. Smith (1987), Compressibility of solids, *J. Geophys. Res.*, *92*(B9), 9319–9325.
Wang, Y., D. J. Weidner, R. C. Liebermann, and Y. Zhao (1994), P–V–T equation of state of (Mg, Fe)SiO_3, *Phys. Earth Planet. Inter.*, *83*, 13–40.
Wolstencroft, M., J. H. Davies, and D. R. Davies (2009), Nusselt–Rayleigh number scaling for spherical shell Earth mantle simulation up to a Rayleigh number of 10^9, *Phys. Earth Planet. Inter.*, *176*(1), 132–141.
Ye, Y., C. Gu, S.-H. Shim, Y. Meng, and Y. Prakapenka (2014), The postspinel boundary in pyrolitic compositions determined in the laser-heated diamond anvil cell, *Geophys. Res. Lett.*, *41*, 3833–3841, doi:10.1002/2014GL060060.
Yokoo, M., N. Kawai, K. G. Nakamura, K. Kondo, Y. Tange, and T. Tsuchiya (2009), Ultrahigh-pressure scales for gold and platinum at pressures up to 550 GPa, *Phys. Rev. B*, *80*(10), 104114.
Yoshida, M., A. Onodera, M. Ueno, K. Takemura, and O. Shimomura (1993), Pressure-induced phase transition in SiC, *Phys. Rev. B*, *48*(14), 10587.
Zhuravlev, K., A. F. Goncharov, S. Tkachev, P. Dera, and V. Prakapenka (2013), Vibrational, elastic, and structural properties of cubic silicon carbide under pressure up to 75 GPa: Implication for a primary pressure scale, *J. Appl. Phys.*, *113*(11), 113503.